

 Open access • Journal Article • DOI:10.1016/J.MSEC.2012.01.019

Porous poly(vinyl alcohol)/sepiolite bone scaffolds: Preparation, structure and mechanical properties — [Source link](#)

Derek Killeen, Martin Frydrych, Biqiong Chen





Institutions: Trinity College, Dublin

Published on: 01 May 2012 - Materials Science and Engineering: C (Elsevier)

Topics: Sepiolite, Nanocomposite, Vinyl alcohol and Ultimate tensile strength

Related papers:

- [Molecular access to intracrystalline tunnels of sepiolite](#)
- [Structure and mechanical properties of gelatin/sepiolite nanocomposite foams](#)
- [Study of silane treatment on poly-lactic acid\(PLA\)/sepiolite nanocomposite thin films](#)
- [Characterization and properties of sepiolite/polyurethane nanocomposites](#)
- [Preparation, structure and thermal properties of polylactide/sepiolite nanocomposites with and without organic modifiers](#)

Share this paper:    

View more about this paper here: <https://typeset.io/papers/porous-poly-vinyl-alcohol-sepiolite-bone-scaffolds-11mrr6bejn>

Accepted Manuscript

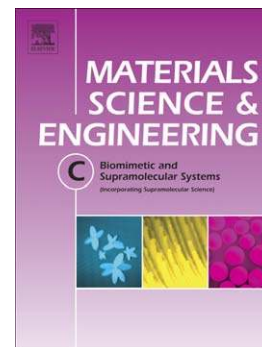
Porous poly(vinyl alcohol)/sepiolite bone scaffolds: preparation, structure and mechanical properties

Derek Killeen, Martin Frydrych, Biqiong Chen

PII: S0928-4931(12)00030-6
DOI: doi: [10.1016/j.msec.2012.01.019](https://doi.org/10.1016/j.msec.2012.01.019)
Reference: MSC 3277

To appear in: *Materials Science & Engineering C*

Received date: 23 July 2011
Revised date: 20 December 2011
Accepted date: 19 January 2012



Please cite this article as: Derek Killeen, Martin Frydrych, Biqiong Chen, Porous poly(vinyl alcohol)/sepiolite bone scaffolds: preparation, structure and mechanical properties, *Materials Science & Engineering C* (2012), doi: [10.1016/j.msec.2012.01.019](https://doi.org/10.1016/j.msec.2012.01.019)

This is a PDF file of an unedited manuscript that has been accepted for publication. As a service to our customers we are providing this early version of the manuscript. The manuscript will undergo copyediting, typesetting, and review of the resulting proof before it is published in its final form. Please note that during the production process errors may be discovered which could affect the content, and all legal disclaimers that apply to the journal pertain.

Porous poly(vinyl alcohol)/sepiolite bone scaffolds: preparation, structure and mechanical properties

Derek Killeen¹, Martin Frydrych^{1,2} and Biqiong Chen^{1,2*}

¹Trinity Centre for Bioengineering, Trinity College Dublin, College Green, Dublin 2, Ireland.

²Department of Mechanical and Manufacturing Engineering, Trinity College Dublin, College Green, Dublin 2, Ireland.

*To whom correspondence should be addressed.

E-mail: chenb@tcd.ie;

Tel: +353 1 896 1729

Fax: +353 1 679 554

Abstract

Porous poly(vinyl alcohol) (PVA)/sepiolite nanocomposite scaffolds containing 0-10wt.% sepiolite were prepared by freeze-drying and thermally crosslinked with poly(arylic acid). The microstructure of the obtained scaffolds was characterised by scanning electron microscopy and micro computer tomography, which showed a ribbon and ladder like interconnected structure. The incorporation of sepiolite increased the mean pore size and porosity of the PVA scaffold as well as the degree of anisotropy due to its fibrous structure. The tensile strength, modulus and energy at break of the PVA solid material that constructed the scaffold were found to improve with additions of sepiolite by up to 104%, 331% and 22% for 6wt.% clay. Such enhancements were attributed to the strong interactions between the PVA and sepiolite, the good dispersion of sepiolite nanofibres in the matrix and the intrinsic properties of the nanofibres. However, the tensile properties of the PVA scaffold deteriorated in the presence of sepiolite because of the higher porosity, pore size and degree of anisotropy. The PVA/sepiolite nanocomposite scaffold containing 6wt.% sepiolite was characterized by an interconnected structure, a porosity of 89.5% and a mean pore size of 79 μ m and exhibited a tensile strength of 0.44MPa and modulus of 14.9MPa, which demonstrates potential for this type of materials to be further developed as bone scaffolds.

Keywords: Poly(vinyl alcohol), nanocomposite, foam, morphology, mechanical properties

1. Introduction

Bone is the umbrella name given to a group of biological materials that share the same basic building block, the mineralised collagen fibril that is utilised to build an array of structures with differing structural motifs that stretch from Ångstroms to millimeters [1–3]. As well as performing the obvious role of mechanical support, bone performs other important functions such as storage of minerals and lipids, production of blood cells and protection for underlying vital organs. Bone is prone to illness, damage and defects as much as any other tissue and is the second most common transplanted tissue after blood [4]. It has been estimated that in the United States alone there are over 6.6 million fractures every year leading to an estimated 550,000 cases requiring grafting [5]. The clinical need for a substitute material has come about due to the shortcomings of current methodologies for treating bone defects, usually involving replacement bone acquired from various sources (autografts, allografts, xenografts and demineralised bone matrix). Although they are considered good therapies, none of these treatments is ideal and all have drawbacks such as acute inflammatory response [6] and donor site morbidity [7], among others. This pressing need for a viable substitute bone graft material has led to much research involving a range of materials, techniques and approaches. As early as the 1920's calcium phosphate was being researched and reported on as a possible bone substitute material [8]. Since then, the overwhelming majority of the research into prospective bone substitutes has dealt largely with materials that are compositionally similar to bone such as calcium phosphates and biopolymers. The search for bone substitutes that fulfill the property/functionality criteria, such as adequately load-bearing, biodegradable, osteoinductive, osteoconductive and ideally simulating bone's own structures and functions, is still ongoing.

In order to realise an effective substitute bone graft material it is necessary to understand the composition, structure and organisational motifs that exist throughout the hierarchical levels in natural bone. The hierarchical structure of bone stems from the most basic building blocks at the nanoscale, namely mineralized collagen nanofibres, their arrangement into microstructures and finally, at the highest level, into types of bone [1]. Such hierarchical structure governs the function of bone and varies with bone type. For example, compact or cortical bone is dense and is found usually when there are uniaxial stresses involved such as the long bones of arms and legs and the hard outer layer of bones, while trabecular or cancellous bone is less dense, spongy in appearance, consisting of a mesh of struts that are subjected to generally lower but more multidirectional stresses such as the interior of bones

[1-3, 9]. The basic components of bone are collagen, dahllite and water, accounting for 50–60%, 30–40% and –10% respectively by weight [10]. These values do fluctuate between various bone types.

The goal of this research was to develop novel biopolymer nanocomposite porous scaffolds that contain natural nanofibres and attempt to mimic the hierarchical structure and mechanical properties of trabecular bones as potential scaffolds for bone tissue engineering.

PVA is a hydrophilic synthetic polymer that possesses excellent recognised biocompatibility and properties such as non-toxicity, non-carcinogenicity, ease of processing and mechanical strength [11-14]. It has been studied as bone substitute material or bone scaffold coating when mixed with ceramics [14-16], a synthetic articular cartilage [17-19], artificial pancreas [20], artificial skins [21,22], and drug delivery systems [23], etc. To improve the stability of PVA in body fluids, glutaraldehyde is often used to crosslink PVA [21]. In this work, a non-toxic hydrophilic polymer, poly(acrylic acid) (PAA), with a low molecular weight, was employed as the crosslinker due to its chain mobility and carboxyl groups that react with the hydroxyl groups in PVA to form an ester [24,25]. Similar to PVA, PAA also displays excellent biocompatibility and has been used in applications such as site-specific drug delivery systems [26,27], wound dressing materials [28] and partially degradable bone cements [29]. It has also been used in conjunction with PVA to form hydrogel fibres where the degree of swelling can be easily controlled by the degree of crosslinking [30].

Sepiolite, $(\text{Si}_{12})(\text{Mg}_8)\text{O}_{30}(\text{OH})_4(\text{OH}_2)_{48}\cdot\text{H}_2\text{O}$, is a natural, crystalline, hydrated magnesium silicate which consists of needle shaped fibres with diameters at the nanoscale [30-32]. It is composed of blocks, which are characterized by a sandwich structure of a central magnesium octahedral sheet between two silica tetrahedral sheets, forming a capillary network of parallel channels [31-33]. Sepiolite features a large specific surface area in the region of 140 - 320 m^2/g [31,34], and its interactions with polymer(s) not only take place on the external surface, due to the significant number of silanol (Si-OH) groups but by penetration into the structural channels of sepiolite fibre blocks [35,36]. Previous studies demonstrated good reinforcing capability of sepiolite in polymeric matrices and such reinforcements were obtained at low sepiolite contents, typically lower than 10wt.% [37,38]. For example, with the presence of 9.1 wt% sepiolite, the compressive modulus and strength of gelatin foam with a cell size of 159 μm and a porosity of 98% were increased by 288% and 308%, respectively. Such enhancements were attributable to the strong interactions between hydrophilic gelatin

and sepiolite, the reduced cell size and the reinforcement effect of sepiolite on the gelatin solid material [38]. The incorporation of sepiolite also enhanced the bioactivity of gelatin film due to its negative surface charge, by inducing more and smaller calcium phosphates on the polymer surface when immersed in a simulated body fluid [38]. Hydroxapatite nanoparticles can grow on the surface of sepiolite nanofibres, revealing bioactivity of the clay on its own [34]. Furthermore, previous research has demonstrated that sepiolite is biocompatible and non-toxic [39,40], indicating a confident use in the biomedical field. Thus, the addition of sepiolite to PVA is expected to reconstruct the nanofibrous structure in bone and to enhance both the mechanical properties and bioactivity of PVA scaffolds.

This paper reports the structure and mechanical properties of PVA/sepiolite nanocomposite foams prepared by freeze-drying for potential uses as trabecular bone scaffolds. The foams were thermally crosslinked in the presence of a small amount of low molecular weight PAA. The structure of the scaffolds was characterised by using scanning electron microscopy (SEM) and micro computer tomography (μ CT), the interactions between the components were investigated by Fourier transform infrared spectroscopy (FT-IR) and the mechanical properties were studied from tensile testing results. PVA/sepiolite films crosslinked with PAA, which correspond to the foam samples, were prepared by solution casting and tested in parallel for fundamental understanding of the mechanical properties of the nanocomposite foams.

2. Materials and methods

2.1 Materials

Poly(vinyl alcohol) (99+% hydrolysed, $M_w=89,000\sim 98,000$ g/mol) and poly(acrylic acid) (50wt.% solution in electric grade water, $M_w=2,000$ g/mol) were purchased from Sigma-Aldrich. A high-purity sepiolite clay (Pansil® S1500) was obtained from Tolsa (Spain).

2.2 Fabrication of nanocomposite films and porous scaffolds

In all the nanocomposite film and scaffold samples, the weight ratio of PVA to PAA was fixed at 93:7, and the contents of sepiolite nanofiller in the nanocomposites were 0%, 2%, 4%, 6%, 8% and 10% by weight (wt.%). These weight percentages were chosen because clay enhancements are typically achieved at loadings below 10wt.% as previously mentioned, and

they represented even distribution of the loadings in order to obtain the optimum clay content for this type of materials. The solutions for fabrication of the nanocomposite films and scaffolds were prepared using the following process: 20g of PVA material was completely dissolved in 200mL of distilled water at 80°C under constant stirring. Sepiolite clay was dried in an oven at 60°C for two hours before use, weighed to the percentage concentration and added to distilled water at room temperature for formation of 3wt.% dispersion by mixing on a rolling table for 1 day. The dispersion was then sonicated for 45 minutes and left on the rolling table again for 2 hours to ensure even dispersion of sepiolite nanofibres in water. After that, 1.506g of PAA was added to the dispersion, followed by a further mixing of 4 hours to allow PAA molecules to be adsorbed onto the clay surface. Finally the PAA/sepiolite dispersion and PVA solution were combined and mixed by magnetic stirring for 4 hours for subsequent uses.

To obtain uncrosslinked nanocomposite films, the PVA/PAA/sepiolite solutions were poured into large petri dishes and placed in an oven at 60°C until the water had evaporated leaving a thin film in the base of the dish with a target thickness of approximately 0.5mm.

The preparation of uncrosslinked nanocomposite porous scaffolds from the PVA/PAA/sepiolite solutions involved the following process. First, the solutions were degassed in a vacuum oven at 60°C for 30 minutes, which were then poured into a stainless steel mould for freeze-drying. Freezing was carried out in a freeze-dryer (FreeZone Triad, Labconco Corp. MO USA), with a cooling rate of 0.9°C min⁻¹ and a final freezing temperature of -40°C. When the temperature of -40°C was reached the samples were held for 3 hours to ensure complete freezing of the contents. Then, the temperature was raised at a rate of 1°C min⁻¹ to -5°C, the set point where the sublimation of the ice crystals began to happen, and held at -5°C for 17 hours before increasing the temperature to 35°C and holding at this temperature for a period of 3 hours to ensure complete drying of the samples.

For crosslinking, all the film and foam samples with varying concentrations of sepiolite were operated under vacuum at 150°C for 30 minutes to improve their stability and mechanical properties according to the methods described in the literature [26, 27, 30]. PAA with a low molecular weight of 2,000 g/mol was chosen as the crosslinking agent due to its chain mobility in PVA, as previously mentioned. The crosslinking reaction between the hydroxyl groups in PVA and the carboxyl groups in PAA to form an ester may not occur if a high molecular weight PAA is used, because of the high inflexibility of the PAA chain in the

PVA network [26]. All the results presented in this work are for crosslinked films and foams, noted as PVA/PAA/sepiolite foams and films with varying sepiolite contents.

2.3 Morphological characterisation

The morphology of the scaffold samples was analysed by using SEM and μ CT. SEM was carried out on a Tescan MIRA–XMU scanning electron microscope using secondary electrons operated with an accelerating voltage of 5kV. Samples were prepared in advance by cutting 2mm sections from the scaffold sheet using a sharp razor blade. They were then mounted to SEM stubs, followed by sputter coating of platinum–palladium of 10nm for improved conductivity during imaging. The morphology of pristine sepiolite nanofibres was also investigated as a control.

μ CT analysis was performed by using a desktop X–ray tomography scanner (μ CT 40, Scanco medical AG, Switzerland). Using an energy of 50kVp, a current of 177 μ A and a spatial resolution of 8 μ m, a homogenous area of approximately 20mm² from the centre of the scaffold was analysed and resulting Voxel data were recorded. Quantitative analysis of the pore size and porosity was obtained from structural indices measured from bone scaffold samples. Total Volume (*TV*) was calculated as the overall volume of the measured sample. Bone scaffold Surface (*BS*) was calculated from triangulation of the scaffold surface while Bone scaffold Volume (*BV*) was calculated using tetrahedrons corresponding to the enclosed volume of the triangulated surface. The sample porosity, *P*, can then be expressed as (1–*BV/TV*). Similarly, strut or pore wall thickness (*Tb.Th*) and trabecular separation or pore size (*Tb.Sp*) were calculated by measurements in the 3D space [41].

The porosity of the bone scaffold or foam, *P*, was also calculated from the density of foam, ρ_f , and the density of film, ρ_s , according to Eq. 1:

$$P = (1 - \rho_f / \rho_s) \times 100\% \quad (1)$$

The density of foam was determined by measuring the volume and mass of a section of foam from each filler concentration. A section of foam of approximately 20mm x 20mm x 5mm in dimensions was cut and the volume was calculated from accurately measured dimensions using a digital microscope (Micropak 5 Mk2, Mitutoyo Japan). The mass was measured using a four–place laboratory balance (AB204–S, Mettler Toledo, Switzerland). This was repeated for three pieces of foam and an average density was acquired.

The density of the solid material (film) was calculated according to the mass fractions (M_x where x refers to the constituent material) and densities of the constituent materials (ρ_x), by assuming the total mass and volume remain the same before and after reaction, using Eq. 2:

$$\rho_s = \frac{M_{sep} + M_{PVA} + M_{PAA}}{(M_{sep}/\rho_{sep}) + (M_{PVA}/\rho_{PVA}) + (M_{PAA}/\rho_{PAA})} \quad (2)$$

The densities of the constituent materials are 1.27Mg m^{-3} , 1.09Mg m^{-3} and 2.38Mg m^{-3} for PVA, PAA and sepiolite, respectively, with the first two taken from the supplier, Sigma-Aldrich, and the last one determined by helium pycnometry using a MicroMeritics AccuPyc 1330 Pycnometer [34].

The dispersion of sepiolite nanofibres in the polymer matrix was characterized by performing SEM and Energy Dispersive X-ray Analysis (EDX) on the polymer and polymer nanocomposite films. Back scattered electron imaging and EDX were carried out on carbon-coated specimens by using the same microscope as above-mentioned, a voltage of 7kV and Oxford INCA software with an Oxford X-Max X-Ray detector.

2.4 Fourier Transform Infrared Spectroscopy

FT-IR was performed on a Perkin Elmer Spectrum One NTS analyzer (resolution 4cm^{-1}) with a wavenumber range of $650\text{--}4000\text{cm}^{-1}$. FT-IR spectra were obtained from PVA, PAA, sepiolite, and the crosslinked polymer and nanocomposite films.

2.5 Tensile testing

Tensile testing was carried out on a Zwick Z050 mechanical tester at ambient temperature (20°C) at a constant speed of 1.6mm min^{-1} . Load cells of 5kN and 50N were used for films and scaffolds respectively, given the differences in their properties. Dog-bone specimens of the shape and size in accordance with ISO 20753:2008 were cut from the films and foams using an aluminum template and used for testing. Before testing the specimens were conditioned by being placed in an oven at 24°C for 4 hours, in accordance with ISO 291:2008. Five specimens were tested for each material. The results are expressed as mean value \pm standard deviation with the confidence level of 95%.

3. Results and discussion

3.1 Morphologies

The densities, porosities and microstructures of the crosslinked PVA/PAA/sepiolite nanocomposite foams containing sepiolite contents from 0wt.% to 10wt.% were investigated by density measurement, SEM and μ CT. Table 1 shows the densities of PVA/PAA/sepiolite nanocomposite foams (ρ_f) and films (ρ_s) as well as the porosities of the foams calculated by Eq. 1. The density of the PVA/PAA foam decreased monotonously with increasing sepiolite content from 0.19Mg m^{-3} to 0.09Mg m^{-3} for the nanocomposite foam containing 10wt.% clay. The density of PVA/PAA film, calculated from Eq. 2, increased slightly by additions of sepiolite due to the higher density of the nanofiller compared to the polymers. The porosity of the PVA/PAA foam was found to increase monotonously with increasing sepiolite content, namely from 84.6% up to 93.2%. Such change does not agree with the results for gelatin/sepiolite foams [38] where the addition of sepiolite did not increase the porosity due to the high starting value of the porosity. However, it is coincident with the general trend for polymer/clay foams that the incorporation of clay enhances the porosity [42,43].

Fig. 1 (a) shows the SEM micrograph of pristine sepiolite, illustrating its unique nanofibrous structure. The sepiolite fibers used in this work has a length of 0.5-5 μm and a width of 17-55nm. This is in accordance with the results from transmission electron microscopy of sepiolite nanofibres reported in our previous work [34]. SEM micrographs of PVA/PAA/sepiolite nanocomposite foams demonstrate that the foam materials are characterised by an interconnected and highly porous structure. Ribbon-like structures can be seen in Fig. 1 (b) and (c), from the neat PVA/PAA foam and the nanocomposite foam with 2wt.% sepiolite. More elongated and directional porous structures are illustrated in Fig. 1 (d) and (e) for foams with 4wt.% and 6wt.% sepiolite, which can be attributed to the nanofibrous structure and high aspect ratio of sepiolite.

At higher magnifications, tubular structured micro and macro pores of various sizes can be seen in for example Fig. 2 for the neat PVA/PAA foam and the nanocomposite foam with 10wt.% sepiolite. The images also revealed an internal ladder-type structure which is typical of polymer foams formed by a thermally induced phase separation method, with channels appearing parallel to the uniaxial direction of solidification (heat transfer direction) [44], while the uniformly spaced pores are largely perpendicular to this direction [45]. This structure is formed by an initial liquid-liquid phase separation forming the vertical channels while localised depletion of the polymer from the solution ahead of an additional phase

separation front leads to the creation of the horizontal tubular pores [46]. Furthermore, the structure for the neat PVA/PAA foam featured much smaller pores compared to the foam with 10wt.% sepiolite clay, which agrees with the results for chitosan/titania and poly(L-lactic) acid/bioglass nanocomposite foams [47,48] but in contradiction to the work for polyurethane/fluor-hydroxyapatite [49], gelatin/sepiolite [38] as well as gelatin/montmorillonite/chitosan nanocomposite foams [50]. Pore size and pore structure are controlled by the ice crystals formed during the freeze-drying process, which are dependent on the freezing and drying conditions (e.g. temperatures and rates), concentration and solute of the solution as well as the material and design of the freeze-drying container [38]. Due to the fact that all PVA/PAA/sepiolite nanocomposite foams were fabricated using the same processing conditions, the difference in the pore size can be ascribed to the presence of sepiolite in the PVA/PAA nanocomposites foams that affects formation and growth of ice crystals.

To expose the 3D internal structure of the PVA/PAA/sepiolite foams, μ CT scans were performed to analyse the effect of sepiolite on the foam structure, as demonstrated in Fig. 3. The results for the pore size, porosity, bone surface to volume ratio (BS/BV), degree of anisotropy (DA), trabecular spacing ($Tb.Sp$) and thickness ($Tb.Th$) were assessed from each foam type, as seen in Table 2. The threshold value, while being subjective, was set at 22 as this reflected the density value that was obtained by direct measurement of the neat foam. As a result, the porosities are similar to the measured values presented in Table 1 and are shown in Table 2 only for verification of the threshold setting.

μ CT results demonstrate that the pore size and the porosity increased with a higher amount of sepiolite from 50 μ m (0wt.% sepiolite) up to 92 μ m (10wt.% sepiolite; rise of 84%) and from 84.4% (0wt.% sepiolite) to a maximum value of 96.2% (8wt.% sepiolite; rise of 14%), respectively. The bone surface to volume ratio increased from 152.4mm⁻¹ (0wt.% sepiolite) to 225.6mm⁻¹ (10wt.% sepiolite) with increasing sepiolite content, which describes an enhancement of 48%. In respect to the geometrical degree of anisotropy (the ratio between the maximum and minimum radii of the ellipsoid fitted to the mean intercept length [51,52]; DA value of 1.0 indicates overall material isotropy), the nanocomposite foams presented similar DA values to that of pristine PVA/PAA foam except for those with 4wt.% and 6wt.% where DA increased from 1.15 to 1.34 and 1.26 respectively showing increased directional porous structures. This finding is coincident with the SEM results as discussed above and is due to the presence of sepiolite nanofibers which may, along with the heat transfer, direct the growth of ice crystals during freeze drying. An increase of the sepiolite content from 6wt.%

to 8wt.% or higher presumably led to poorer dispersion of sepiolite nanofibres in PVA/PAA, thus decreasing the value of DA. The trabecular spacing (average of all non-material parts of the foam which are filled with maximum spheres to estimate a mean value [53]) increased with increasing sepiolite content from 55 μm (0wt.% sepiolite) to a maximum value of 97.9 μm (8wt.% sepiolite; rise of 78%), while the trabecular thickness (average of all material parts of the foam which are filled with maximum spheres to estimate a mean value [53]) decreased from 21 μm (0wt.% sepiolite) to a maximum of 15.8 μm (10wt.% sepiolite; decline of 25%).

Table 2 and Fig. 3 clearly show that the increasing addition of sepiolite clay had a profound effect on the foaming process, leading to more porous foams with larger pore sizes, decreased strut thickness and increased specific surface area. For instance, the neat PVA/PAA foam featured the lowest pore size, porosity and specific surface area while these parameters increased with increasing sepiolite content, with 10wt.% addition displaying the largest pore size, one of the highest porosity and the largest measured specific surface area. The fact that the bone surface to volume ratio increased with the higher amount of sepiolite in general, indicates that the specific cell surface area of the open-cell foams rose. As a result, the trabecular spacing enhanced and trabecular strut thickness reduced. Regarding the geometrical degree of anisotropy, the data obtained from each scan revealed that the longest axis of the pores was in the z or vertical axis, in keeping with the results obtain from SEM images.

3.2 Interfacial interactions

FT-IR spectra of the PVA/PAA/sepiolite nanocomposite films are shown in Fig. 4. The results illustrate that the characteristic bands of the PVA/PAA shifted with the additions of sepiolite. The O-H stretching band for the neat PVA/PAA at 3270 cm^{-1} increased slightly to 3272 cm^{-1} for 2wt.% and 4wt.% sepiolite but reduced to 3267 cm^{-1} for 6wt.% and 8wt.% and further to 3257 cm^{-1} for 10wt.% sepiolite addition. Such shifts indicate the formation of hydrogen bonds between the silanol groups (Si-OH) on the sepiolite surface and the hydroxyls of PVA, demonstrating strong interactions between the polymers and the clay [54] and hence positively influencing the mechanical properties as discussed below. Furthermore, the peak designated to C-O stretching mode moved from 1086 cm^{-1} to 1071 cm^{-1} , in relation to the neat PVA/PAA and the PVA/PAA/sepiolite nanocomposite with 10wt.% sepiolite, again due to formation of hydrogen bonds with the Si-OH groups on the sepiolite surface.

The introduction of two new peaks to the spectrum of the PVA/PAA can be seen for the PVA/PAA/sepiolite nanocomposites with 6wt.%, 8wt.% and 10wt.% sepiolite. The peak at 980cm^{-1} can be assigned to the stretching of Si–O bonds of the pristine sepiolite, while the peak at $1021\text{--}1028\text{cm}^{-1}$ is related to Si–O–Si in-plane vibration [55]. Variations in the latter peak further indicate strong interactions between sepiolite and PVA/PAA. The interactions between sepiolite and PVA/PAA, via formation of hydrogen bonds, are depicted in Scheme 1. This scheme was drawn based on the reaction mechanisms proposed by Rhim et al. [24] for thermally crosslinked PVA/PAA but also taking into account the residual hydroxyl bonds presented on PVA owing to the shorter crosslinking time.

3.3 Mechanical properties

To investigate the reinforcement mechanisms in the nanocomposite foams, the nanocomposite films that have the same compositions as in the foams were tested and considered as the materials construct the cell surfaces, edges and walls. Table 3 illustrates the average values of the Young's modulus, tensile strength, elongation at break and energy at break for all PVA/PAA/sepiolite nanocomposite film samples. The results for the Young's modulus were calculated from stress-strain graphs using strains of $\epsilon = 0.0005$ and 0.0025 in the initial linear zone in accordance with ISO 527–1:1996. The Young's modulus increased with increasing clay concentration from 111.0MPa (0wt.% sepiolite), by a maximum of 327% (8wt.% sepiolite), to a value of 474.2MPa. At a higher sepiolite content (10wt.% sepiolite) the Young's modulus decreased to 216.4MPa. The tensile strength also increased with increasing sepiolite content from 19.0MPa (0wt.% sepiolite) by a maximum of 103% (6wt.% sepiolite), to a value of 38.7MPa. At higher sepiolite contents a tendency of deterioration can be seen in which the tensile strength decreased to a minimum of 16.1MPa (10wt.% sepiolite). Decrease in the tensile strength supports the previous hypothesis of poorer dispersion of the nanofibres in PVA/PAA at higher filler contents, which hinders effective stress transfer. The elongation of the film samples decreased with higher sepiolite contents from a maximum of 329% (0wt.% sepiolite) to a minimum of 101% (10wt.% sepiolite), resulting in more brittle materials. The results of the energy at break (calculated as the area under the curve on the stress-strain graph) indicate no tendency and oscillate around a value of $900\text{--}1200\text{MJ m}^{-3}$, for samples which contain 0–8wt.% sepiolite content. At a

higher sepiolite content (10wt.% sepiolite) a significantly lower value was measured, of only 261.7MJ m^{-3} , suggesting catastrophic reduction in toughness.

The results showed that the best overall mechanical properties were achieved at a sepiolite content of 6wt.%. At higher sepiolite concentrations the results showed a tendency of deterioration which may be explained by the aggregation of clay particles, leading to possible stress concentrators and a resultant reduction in the mechanical properties.

Such a hypothesis about clay distribution was verified by the results from SEM and EDX on polymer and polymer nanocomposite films which are depicted in Fig.6. With backscattered SEM, the organic matrix and inorganic filler were clearly distinguished on the images, with the latter shown as white particles. This was confirmed by the EDX spectrum on the clay nanofibre (Fig.6b1) which demonstrated the elements of Si, Mg and O, characteristic of sepiolite. The presence of Al on the spectrum was mainly due to the aluminium sample stub, and the small peak assigned to Fe may be attributed to the impurity in the as-received sepiolite. No particles were detected on the image for the unfilled PVA/PAA (Fig. 6a). When the clay content was 6wt.% (Fig.6b), white particles with sizes typically smaller than $5\mu\text{m}$ and similar to the lengths of sepiolite nanofibres were uniformly distributed in the polymer matrix, indicating good dispersion of nanofibres at this clay loading. In contrast, agglomerates of particles with sizes up to $38\mu\text{m}$ were visible on the image for the PVA/PAA/sepiolite when the inorganic filler was of 10wt.% (Fig.6c), suggesting poorer dispersion of the filler.

The tensile testing results confirm clearly the FT-IR analysis, which indicates strong interactions between the PVA/PAA matrix and sepiolite, influencing the overall mechanical properties of the PVA/PAA film samples. The results also ratify previous work of polymer-clay nanocomposites [38, 56-60] that show significant enhancement of the mechanical properties of the polymer based on the good dispersion of sepiolite in the polymer matrix at low clay contents, the strong interactions between the components, and the intrinsic properties of sepiolite nanofibres such as a high strength, modulus and specific surface area [34].

Table 4 demonstrates the mean and standard deviation values of the Young's modulus, tensile strength, elongation at break and energy at break for all the PVA/PAA/sepiolite nanocomposite foams prepared. The highest values of 29.9MPa and 0.85MPa for the Young's modulus and tensile strength were achieved by the PVA/PAA foam without clay. With additions of sepiolite, both the Young's modulus and tensile strength were decreased with the nanocomposite foams containing 8wt.% and 10wt.% sepiolite exhibiting the lowest

values. In contrast, the nanocomposite foam with 8wt.% sepiolite obtained the highest elongation at break, demonstrating an increase of 64% in respect to the neat PVA/PAA foam. The foams with 2wt.% and 4wt.% clay also showed increased values of elongation at break while those containing 6wt.% and 10wt.% clay presented decreases of 14% and 24%, respectively. The energy at break results indicate a tendency of deterioration with higher amounts of sepiolite, from 1.62MJ m^{-3} (0wt.% sepiolite) to a minimum of 0.47MJ m^{-3} (10wt.% sepiolite) respectively.

These results illustrate that with increasing sepiolite content the Young's modulus and tensile strength decreased, while the elongation at break increased with exceptions for foam samples with 6wt.% and 10wt.% sepiolite. Overall, the neat PVA/PAA foam exhibited the best mechanical properties and the additions of sepiolite deteriorated the mechanical properties. These results can be partially explained by the fact that the PVA/PAA/clay nanocomposite foams have a higher porosity and pore size compared to those of the neat PVA/PAA foam, as seen in Tables 1 and 2. Both factors induced a reduction of the effective cross-sectional area, therefore destructing the mechanical properties of the neat foam.

In order to eliminate the effect of porosity or foam density, it is necessary to analyse the specific Young's modulus (modulus over density) and specific tensile strength (strength over density), which are presented in Fig. 5. The highest specific Young's modulus and tensile strength of $155\text{MPa (Mg m}^{-3})^{-1}$ and $4.4\text{MPa (Mg m}^{-3})^{-1}$ were calculated for the neat PVA/PAA foam, respectively. The lowest specific Young's modulus and tensile strength with values of only $58\text{MPa (Mg m}^{-3})^{-1}$ and $2.2\text{MPa (Mg m}^{-3})^{-1}$ were obtained for the PVA/PAA/sepiolite nanocomposite foam with 8wt.% sepiolite content, respectively. The nanocomposite foam with 6wt.% sepiolite presented the best specific properties among all the nanocomposite foams investigated, i.e. containing 2-10wt.% clay.

As determined from the mechanical properties of the nanocomposite films, the additions of sepiolite improve the Young's modulus and tensile strength substantially with the exception of 10wt.% clay. This means the solid materials that construct the foams containing 2-8wt.% sepiolite, namely the cell walls and faces, were stiffer and stronger than that for the neat PVA/PAA foam. It can be assumed, that if all foams have the same pore size and pore structure the nanocomposite foams would have better mechanical properties compared to the neat polymer foam. Thus, the reductions in the specific modulus and specific strength can be attributed in part to the greater pore sizes. As shown in Fig. 5 and discussed previously, the presence of sepiolite gave rise to a significantly larger pore size. Interestingly, despite the nanocomposite foam with 6wt.% sepiolite presented higher specific stiffness and strength

than 2wt.% and 4wt.% clay, it had a greater pore size which is beneficial for potential cell growth and penetration in bone tissue engineering, particularly for trabecular bone replacements. In addition to the pore size, the direction of tensile testing in respect to the orientation of pores could also affect the mechanical properties. Tensile testing was carried out perpendicular to the direction of elongated pores or internal ladders. Hence, a higher degree of anisotropy is perceived to affect the mechanical properties more adversely. This, together with pore size, can be used to explain the fact that 4wt.% foam exhibited lower specific properties than 2wt.% foam. Despite the adverse effects from the degree of anisotropy and pore size, the observation that 6wt.% nanocomposite foam gave better mechanical properties than 2wt.% foam is originated from the remarkably higher modulus and strength of the solid material that constructs the foam, being 432.9MPa versus 177.9MPa and 38.7MPa versus 25.5MPa (Table 3). The good combination of the porous structure and mechanical properties for the nanocomposite foam containing 6wt.% sepiolite suggests this type of materials have potential to be further developed into trabecular bone scaffolds by for example changing the material composition and freeze-drying conditions. A biodegradable and biological polymer such as chitosan [14] or bacterial cellulose nanofibres [61] could be incorporated to enhance the biodegradability of the crosslinked PVA/sepiolite scaffolds. To confirm the biocompatibility of these scaffolds, cell culture work should be carried out.

4. Conclusions

Porous PVA/sepiolite nanocomposite scaffolds containing 0-10wt.% sepiolite nanofibres were fabricated by the use of a freeze-drying process and crosslinked with a small amount of a low molecular weight PAA. The scaffolds exhibited a ribbon and ladder like foam structure with tubular micro and macro pores perpendicular to the channels. The addition of sepiolite altered the degree of anisotropy due to its fibrous structure, and increased the average pore size from 50 μ m (0wt.% sepiolite) to 92 μ m (10wt.% sepiolite) and the porosity from 84.6% to 93.2%. FT-IR results suggested strong interfacial interactions by forming hydrogen bonding between the silanol groups on sepiolite surface and the hydroxyls of PVA. Such strong interactions were verified by the significant improvement on the tensile strength of the PAA-crosslinked PVA solid material from 19.0MPa up to 38.7MPa that originated from uniform distribution of sepiolite nanofibres at a content no higher than 6wt.%. The Young modulus and energy at break were simultaneously increased by 331% and 22%, respectively.

However, the mechanical properties of the nanocomposites foams made from the same materials were found to deteriorate with sepiolite additions, attributable to the higher porosity, pore size and degree of anisotropy. By eliminating the porosity, the nanocomposite foam with 6wt.% sepiolite presented the best mechanical properties among all the nanocomposite foams investigated (containing 2-10wt.% sepiolite). This particular PAA-crosslinked PVA/sepiolite foam had a Young's modulus of 14.9MPa, a tensile strength of 0.44MPa and elongation at break of 12.7% as well as a porosity of 89.5% and an average pore size of 79 μ m, demonstrating potential for being further investigated and optimized for applications as bone scaffolds.

Acknowledgements

We thank the Trinity Centre for Bioengineering for financial support of this work. Mr. Peter O'Reilly is thanked for help with tensile testing and μ CT, Dr. Manuel Ruether (Chemistry) is thanked for help with FT-IR, and the staff members at the Centre for Microscopy and Analysis are thanked for their help with SEM and EDX.

References

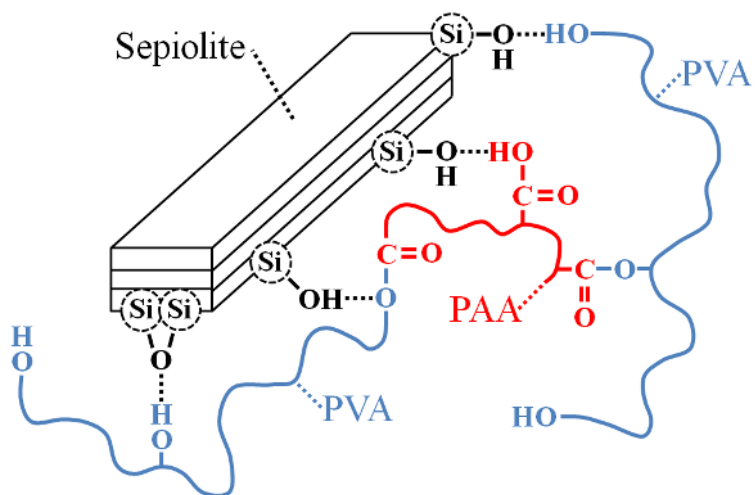
- [1] S. Weiner, H. D. Wagner, The material bone: structure-mechanical function relations, *Annu. Rev. Mater. Sci.* 28 (1998) 271–298.
- [2] S. Weiner, W. Traub, Bone structure: from angstroms to microns, *FASEB J.* 6 (1992) 879–885.
- [3] J.-Y. Rho, L. Kuhn-spearing, P. Zioups, Mechanical properties and the hierarchical structure of bone, *Med. Eng. Phys.* 20 (1998) 92–102.
- [4] H. Shegarfi, O. Reikeras, Bone transplantation and immune response, *J. Orthop. Surg.* 17 (2009) 206–211.
- [5] R. Murugan, S. Ramakrishna, Development of nanocomposites for bone grafting, *Composite. Sci. Technol.* 65 (2005) 2385–2406.
- [6] V.M. Goldenberg, S. Stevenson, Natural history of autografts and allografts, *Clin. Orthop. Relat. Res.* 225 (1987) 7–16.
- [7] P.V. Giannoudis, H. Dinopoulos, E. Tsiridis, Bone substitutes: an update, *Injury* 36S (2005) 20–27.

- [8] F.H. Albee, Studies in bone growth. Triple calcium phosphate as a stimulus to osteogenesis, *Ann. Surg.* 71 (1920) 32–36.
- [9] R. Brand, L. Claes, Book Review: The Law Of Bone Remodeling. *J. Biomech.* 22 (1989)185-187, 1989.
- [10] S.V. Dorozhkin, M. Epple, Biological and medical significance of calcium phosphates, *Angew. Chem. Int. Ed.* 41 (2002) 3130–3146.
- [11] B. Sarti, M. Scandola, Viscoelastic and thermal properties of collagen/poly(vinyl alcohol) blends, *Biomaterials* 16 (1995) 785–792.
- [12] T. Noguchi, T. Yamamuro, M. Oka, Poly(vinyl alcohol) hydrogel as an artificial articular cartilage: evaluation of biocompatibility, *J. Appl. Biomater.* 2 (1991) 101–107.
- [13] Y.L. Li, K.G. Neoh, E.T. Kang, Poly(vinyl alcohol) hydrogel fixation on poly(ethylene terephthalate) surface for biomedical application, *Polymer* 45 (2004) 8779–8789.
- [14] H.S. Mansur, H.S. Costa, Nanostructured poly(vinyl alcohol)/bioactive glass and poly(vinyl alcohol)/chitosan/bioactive glass hybrid scaffolds for biomedical applications, *Chem. Eng. J.* 137 (2008) 72–83
- [15] H.S. Costa, A.A. P. Mansur, E.F. Barbosa-Stancioli, M.M. Pereira, H.S. Mansur, Morphological, mechanical, and biocompatibility characterization of macroporous alumina scaffolds coated with calcium phosphate/PVA, *J. Mater. Sci.* (2008) 43:510–524
- [16] Y. Ma, Y. Zheng, X. Huang, T. Xi, X. Lin, D. Han, W. Song, Mineralization behavior and interface properties of BG–PVA/bone composite implants in simulated body fluid, *Biomed. Mater.* 5 (2010) 025003.
- [17] G. Wu, B. Su, W. Zhang, C. Wang, In vitro behaviors of hydroxyapatite reinforced polyvinyl alcohol hydrogel composite, *Mater. Chem. Phys.* 107 (2008) 364–369.
- [18] H. Bodugoz–Senturk, C.E. Macias, J.H. Kung, O.K. Muratoglu, Poly(vinyl alcohol)–acrylamide hydrogels as load-bearing cartilage substitute, *Biomaterials* 30 (2009) 589–596.
- [19] M. Oka, Biomechanics and repair of articular cartilage, *J. Orthop. Sci.* 6 (2001) 448–456.
- [20] K. Burczak, T. Fujisato, M. Hatada, Y. Ikada, Protein permeation through polymer membranes for hybrid-type artificial pancreas, *Proc. Jpn. Acad.* 67 (1991) 83–88.
- [21] E.S. Costa-Júnior, E.F. Barbosa-Stancioli, A.A.P. Mansur, W.L. Vasconcelos, H.S. Mansur, Preparation and characterization of chitosan/poly(vinyl alcohol) chemically crosslinked blends for biomedical applications, *Carbohydr. Polym.* 76 (2009) 472–481.

- [22] E.S. Costa-Júnior, M.M. Pereira, H.S. Mansur, Properties and biocompatibility of chitosan films modified by blending with PVA and chemically crosslinked, *J. Mater. Sci: Mater. Med.* 20 (2009) 553–561.
- [23] H.S. Mansur, C.M. Sadahira, A.N. Souza, A.A.P. Mansur FTIR spectroscopy characterization of poly (vinyl alcohol) hydrogel with different hydrolysis degree and chemically crosslinked with glutaraldehyde. *Mater.Sci. Eng. C* 28 (2008) 539–548.
- [24] J.W. Rhim, M.Y. Sohn, H.J. Joo, K.H. Lee, Pervaporation separation of binary organic-aqueous liquid mixtures using crosslinked PVA membranes. I. Characterization of the reaction between PVA and PAA, *J. Appl. Polym. Sci.* 50 (1993) 679–684.
- [25] K. Kumeta, I. Nagashima, S. Matsui, K. Mizoguchi, Crosslinking reaction of poly(vinyl alcohol) with poly(acrylic acid) (PAA) by heat treatment: Effect of neutralization of PAA, *J. Appl. Polym. Sci.* 90 (2003) 2420–2427.
- [26] R.G. Riley, K.L. Green, J.D. Smart, J. Tsibouklis, F.C. Hampson, G. Kelly, J.A. Davis, P.W. Dettmar, W.R. Wilber, The gastrointestinal transit profile of ¹⁴C-labelled poly(acrylic acids): an in vivo study, *Biomaterials* 22 (2001) 1861–1867.
- [27] Y. Hu, X. Jiang, H. Ge, Y. Yuan, C. Yang, Synthesis and characterization of chitosan-poly (acrylic acid) nanoparticles, *Biomaterials* 23 (2002) 3193–3201.
- [28] S. Tanodekaew, M. Prasitsilp, S. Swadison, B. Thavornnyutikarn, T. Pothsree, R. Pateepasen, Preparation of acrylic chitin for wound dressing application, *Biomaterials* 25 (2004) 1453–1460.
- [29] I. Espigares, C. Elvira, J.F. Mano, B. Wazquez, J.S. Roman, R.L. Reis, New partially degradable and bioactive acrylic bone cements based on starch blends and ceramic fillers, *Biomaterials* 23 (2002) 1883–1895.
- [30] J. Fei, Z. Zhang, L. Zhong, L. Gu, PVA/PAA Thermo-Induced Hydrogel Fiber: Preparation and pH-Sensitive Behavior in Electrolyte Solution, *J. Appl. Polym. Sci.*, 85 (2002) 2423–2430.
- [31] P. Aranda, R. Kun, M. A. Martín-Luengo, S. Letaïef, I. Dékány, E. Ruiz-Hitzky, Titania–Sepiolite Nanocomposites Prepared by a Surfactant Templating Colloidal Route, *Chem. Mater.*, 20 (2008) 84-91.
- [32] J. Santaren, J. Sanz and E. Ruiz-Hitzky, Structural fluorine in sepiolite, *Clays Clay Miner.*, 38 (1990) 63-68.
- [33] M. Rautureau and A. Mifsud, Electron-microscopy of different hydration states of sepiolite, *Clay Miner.*, 12 (1977) 309-318.
- [34] C. Wan, B. Chen, Synthesis and characterization of biomimetic hydroxyapatite/sepiolite nanocomposites, *Nanoscale* 3 (2011) 693–700.

- [35] S. Inagaki, Y. Fukushima and M. Miyata, Inclusion polymerization of isoprene in the channels of sepiolite, *Res. Chem. Intermed.*, 21 (1995) 167-180.
- [36] E. Ruiz-Hitzky, Molecular access to intracrystalline tunnels of sepiolite, *J. Mater. Chem.*, 11 (2001) 86-91.
- [37] M. Darder, M. López-Blanco, P. Aranda, A. J. Aznar, J. Bravo, E. Ruiz-Hitzky, Microfibrous Chitosan–Sepiolite Nanocomposites, *Chem. Mater.*, 18 (2006) 1602-1610.
- [38] M. Frydrych, C. Wan, R. Stengler, K.U. O’Kelly, B. Chen, Structure and mechanical properties of gelatin/sepiolite nanocomposite foams, *J. Mater. Chem.* 21 (2011) 9103–9111.
- [39] D. B. Warheit, C. M. Sayes, S. R. Frame and K. L. Reed, Pulmonary exposures to Sepiolite nanoclay particulates in rats: Resolution following multinucleate giant cell formation, *Toxicol. Lett.*, 192 (2010) 286-293.
- [40] M. A. Lizarbe, N. Olmo and J. G. Gavilanes, Outgrowth of fibroblasts on sepiolite collagen complex, *Biomaterials*, 8 (1987) 35-37.
- [41] L.M. Mathieu, T.L. Mueller, P.E. Bourban, D.P. Pioletti, R. Mueller, J.A.E. Manson, Architecture and properties of anisotropic polymer composite scaffolds for bone tissue engineering, *Biomaterials* 27 (2006) 905–916.
- [42] X. Cao, L. J. Lee, T. Widya and C. Macosko, Polyurethane/clay nanocomposites foams: processing, structure and properties, *Polymer* 46 (2005) 775–783.
- [43] M. Thirumal, D. Khastgir, N. K. Singha, B. S. Manjunath and Y. P. Naik, Effect of a nanoclay on the mechanical, thermal and flame retardant properties of rigid polyurethane foam, *J. Macromol. Sci., Part A: Pure Appl. Chem.* 46 (2009), 704–712.
- [44] V. Maquet, A.R. Boccacchi, L. Pravata, I. Notingher, R. Jerome, Porous poly(alpha-hydroxyacid)/Bioglass composite scaffolds for bone tissue engineering. I: Preparation and in vitro characterisation, *Biomaterials* 25 (2004) 4185–4194.
- [45] R.Y. Zhang, P.X. Ma, Poly(alpha-hydroxyl acids) hydroxyapatite porous composites for bone-tissue engineering. I. Preparation and morphology, *J. Biomed. Mater. Res.* 44 (1999) 446–455.
- [46] L.L. Whinnery, W.R. Enen, J.V. Beach, D.A. Loy, Engineering the macrostructure of thermally-induced phase-separated polysilane foams, *J. Polymer Sci. Polymer Chem.* 34 (1996) 1623–1627.
- [47] L. Zhao, J. Chang, W. Zhai, Preparation and HL-7702 cell functionality of titania/chitosan composite scaffolds, *J Mater Sci: Mater. Med.* 20 (2009) 949–957.
- [48] N. Barroca, A.L. Daniel-da-Silva, P.M. Vilarinho, M.H.V. Fernandes, Tailoring the morphology of high molecular weight PLLA scaffolds through bioglass addition, *Acta Biomater.* 6 (2010) 3611–3620.

- [49] A. Asefnejad, A. Behnamghader, M.T. Khorasani, B. Farsadzadeh, Polyurethane/fluor-hydroxyapatite nanocomposite scaffolds for bone tissue engineering. Part I: morphological, physical, and mechanical characterization, *Int. J. Nanomedicine* 6 (2011) 93–100.
- [50] J.P. Zheng, C.Z. Wang, X.X. Wang, H.Y. Wang, H. Zhuang, K.D. Yao, Preparation of biomimetic three-dimensional gelatin/montmorillonite–chitosan scaffold for tissue engineering, *React. Funct. Polym.* 67 (2007) 780–788.
- [51] T.P. Harrigan, R.W. Mann, Characterization of microstructural anisotropy in orthotropic materials using a second rank tensor, *J. Mater. Sci.* 19 (1984) 761–767.
- [52] W.J. Whitehouse, The quantitative morphology of anisotropic trabecular bone, *J. Microscopy* 101 (1974) 153–168.
- [53] T. Hildebrand, P. Ruegsegger, A new method for the model-independent assessment of thickness in three-dimensional images, *J. Microscopy* 185 (1997) 67–75.
- [54] M. Alkan, R. Benlikaya, Poly(vinyl alcohol) nanocomposites with sepiolite and heat-treated sepiolites, *J. Appl. Polym. Sci.* 112 (2009) 3764–3774.
- [55] M.A. Vicente–Rodriguez, M. Suarez, M.A. Banares–Munoz, J.D. Lopez–Gonzalez, Comparative FT-IR study of the removal of octahedral cations and structural modifications during acid treatment of several silicates, *Spectrochim. Acta. A* 52 (1996) 1685–1694.
- [56] H. Chen, M. Zheng, H. Sun, Q. Jia, Characterization and properties of sepiolite/polyurethane nanocomposites, *Mater. Sci. Eng. A* 445 (2007) 725–730.
- [57] Y.P. Zheng, Y. Zheng, Study on sepiolite-reinforced polymeric nanocomposites, *J. Appl. Polym. Sci.* 99 (2006) 2163–2166.
- [58] L. Bokoza, A. Burr, G. Garnaud, M.Y. Perrin, S. Pagnotta, Fibre reinforcement of elastomers: nanocomposites based on sepiolite and poly(hydroxyethyl acrylate), *Polym. Int.* 53 (2004) 1060–1065.
- [59] F.M. Fernandes, A.I. Ruiz, M. Darder, P. Aranda, E. Ruiz-Hitzky, Gelatin-clay bio-nanocomposites: structural and functional properties as advanced materials, *J. Nanosci. Nanotechnol.* 9 (2010) 221-229.
- [60] F. Chivrac, E. Pollet, M. Schmutz, L. Averous, Starch nano-biocomposites based on needle-like sepiolite clays, *Carbohydr. Polym.* 80 (2010), 145-153.
- [61] S. Liu, S. Jeannes, B. Chen, Nanofibrous Bacterial Cellulose/Chitosan Scaffolds: Preparation, Structure and Mechanical Properties, *J. Biomater. Tissue Eng.* 1 (2011) 60-67.



Scheme 1. Illustration of the interactions between sepiolite nanofibre and thermally crosslinked PVA/PAA.

Figure captions

Figure 1. SEM micrographs of pristine sepiolite (Scale bar: 300nm) and PVA/PAA/sepiolite nanocomposite foams with various sepiolite contents: (a) 0wt.%, (b) 2wt.%, (c) 4wt.%, (d) 6wt.% and (e) 10wt.% (Scale bar: 100 μ m).

Figure 2. SEM micrographs of PVA/PAA sepiolite nanocomposite foams with (a) 0% and (b) 10wt.% sepiolite. Scale bar: 50 μ m.

Figure 3. Three dimensional μ CT images of PVA/PAA/sepiolite nanocomposite foam sections (a1–f1) and thin cross sections (a2–f2) for foams with 0wt.% (a1, a2), 2wt.% (b1, b2), 4wt.% (c1, c2), 6wt.% (d1, d2), 8wt.% (e1, e2) and 10wt.% (f1, f2) sepiolite. Scale bar: 200 μ m.

Figure 4. FT–IR spectra of PVA/PAA/sepiolite nanocomposite films with (a) 0wt.%, (b) 2wt.%, (c) 4wt.%, (d) 6wt.%, (e) 8wt.% and (f) 10wt.% sepiolite. The FT–IR spectra were shifted vertically for clarity.

Figure 5. Specific Young's modulus and specific tensile strength for PVA/PAA/sepiolite nanocomposite foams with various sepiolite contents.

Figure 6. SEM micrographs of the PVA/PAA/sepiolite nanocomposite films with (a) 0wt%, (b) 6wt% (Square marks the EDX test area) and (c) 10wt% sepiolite (Scale bar: 200 μ m). (b1) EDX graph of sepiolite, taken from the sepiolite block as seen in the SEM micrograph (Scale bar: 2 μ m).

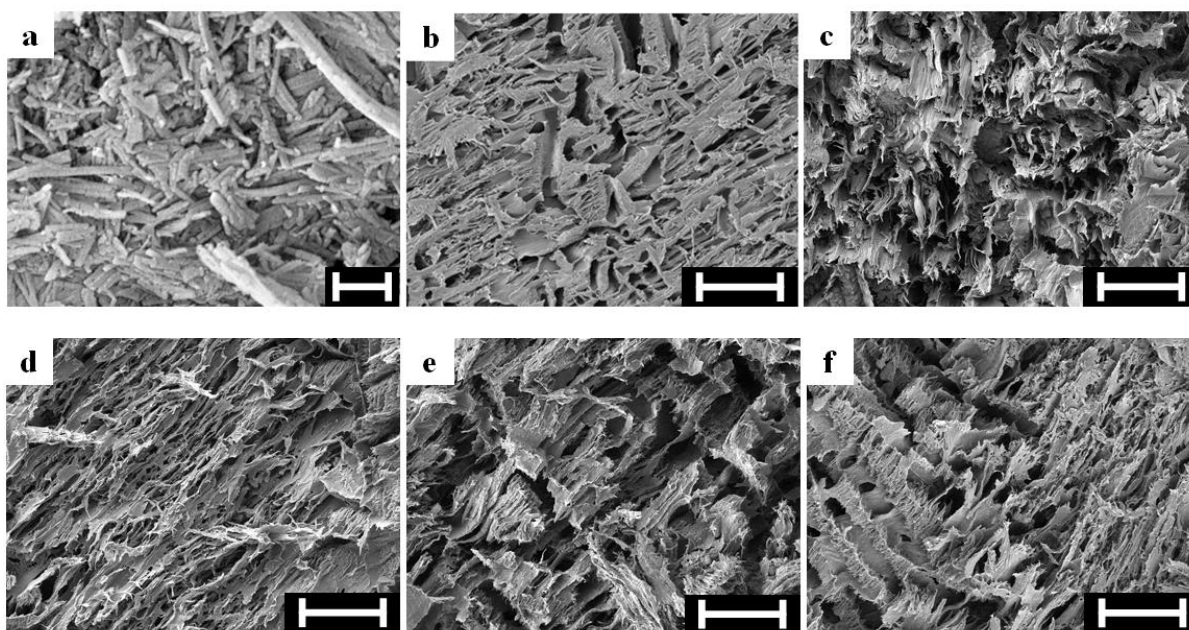


Figure 1. SEM micrographs of pristine sepiolite (Scale bar: 300nm) and PVA/PAA/sepiolite nanocomposite foams with various sepiolite contents: (a) 0wt.%, (b) 2wt.%, (c) 4wt.%, (d) 6wt.% and (e) 10wt.% (Scale bar: 100 μ m).

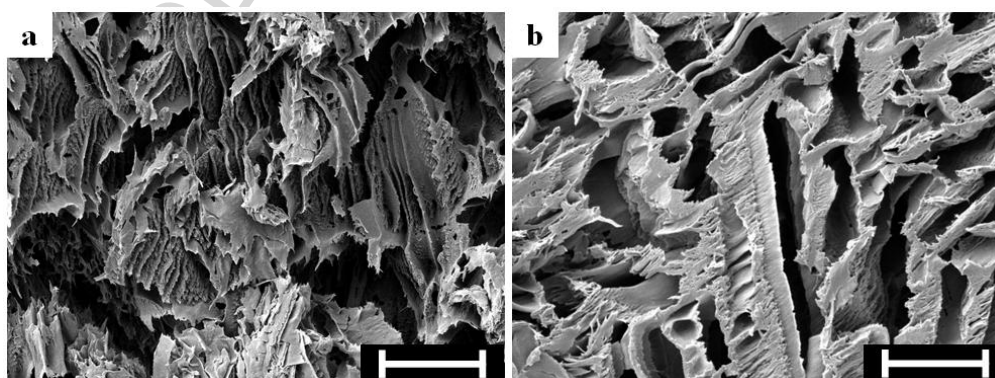


Figure 2. SEM micrographs of PVA/PAA sepiolite nanocomposite foams with (a) 0% and (b) 10wt.% sepiolite. Scale bar: 50 μ m.

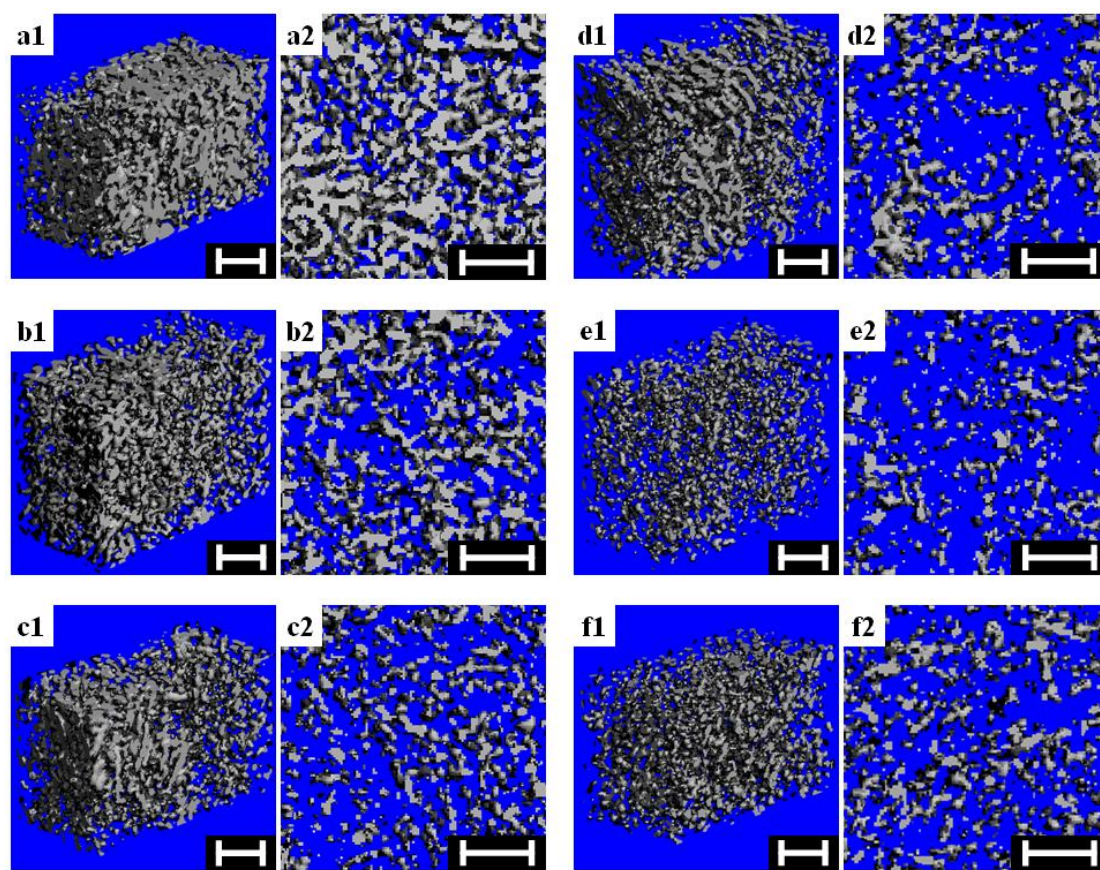


Figure 3. Three dimensional μ CT images of PVA/PAA/sepiolite nanocomposite foam sections (a1–f1) and thin cross sections (a2–f2) for foams with 0wt.% (a1, a2), 2wt.% (b1, b2), 4wt.% (c1, c2), 6wt.% (d1, d2), 8wt.% (e1, e2) and 10wt.% (f1, f2) sepiolite. Scale bar: 200 μ m.

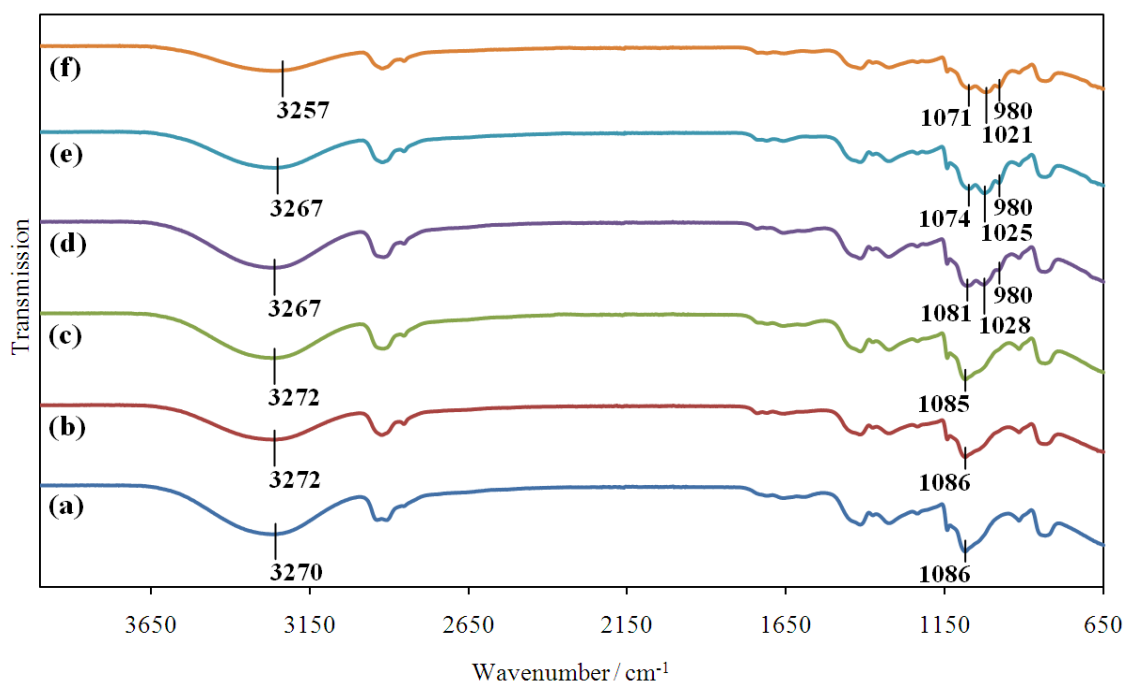


Figure 4. FT-IR spectra of PVA/PAA/sepiolite nanocomposites films with (a) 0wt.%, (b) 2wt.%, (c) 4wt.%, (d) 6wt.%, (e) 8wt.% and (f) 10wt.% sepiolite. The FT-IR spectra were shifted vertically for clarity.

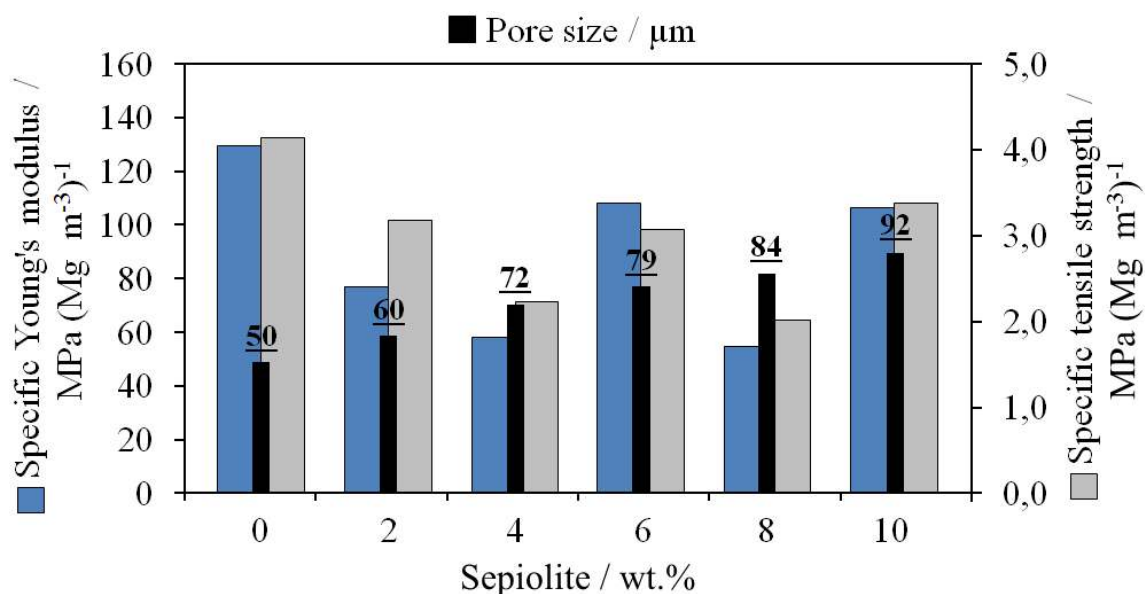


Figure 5. Specific Young's modulus and specific tensile strength for PVA/PAA/sepiolite nanocomposite foams with various sepiolite contents.

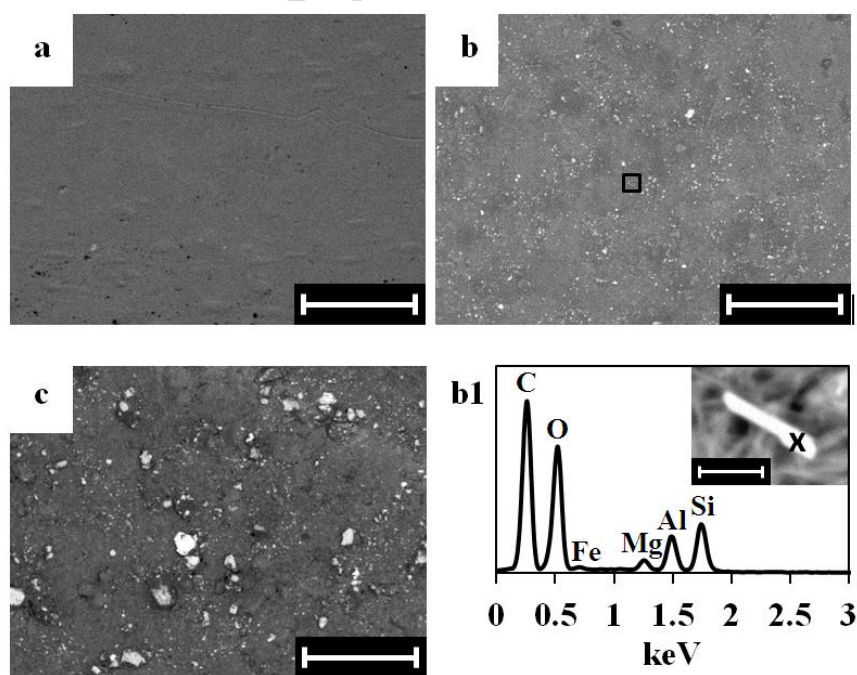


Figure 6. SEM micrographs of the PVA/PAA/sepiolite nanocomposite films with (a) 0wt%, (b) 6wt% (Square marks the EDX test area) and (c) 10wt% sepiolite (Scale bar: 200μm). (b1) EDX graph of sepiolite, taken from the sepiolite block as seen in the SEM micrograph (Scale bar: 2μm).

Table 1. Densities of PVA/PAA/sepiolite nanocomposite foams and their corresponding porosities.

Sepiolite content / wt. %	Foam Density (ρ_f) / Mg m ⁻³	Solid Density (ρ_s)^a / Mg m ⁻³	Porosity (P) / %
0	0.19	1.26	84.6
2	0.16	1.27	87.3
4	0.16	1.28	87.8
6	0.14	1.29	89.5
8	0.10	1.31	92.2
10	0.09	1.32	93.2

^a The density of the solid material that constructs the foam which is calculated from Eq. 2.

Table 2. The structural parameters of PVA/PAA/sepiolite nanocomposite foams obtained from μ CT. (A)

Sepiolite content / wt. %	Porosity / %	Bone surface			Trabecular spacing (<i>Tb.Sp</i>) / μ m	Trabecular thickness (<i>Tb.Th</i>) / μ m
		Pore size / μ m	to volume ratio (<i>BS/BV</i>) / mm ⁻¹	Degree of anisotropy (<i>DA</i>)		
0	84.4	50	152.4	1.15	55.0	21.0
2	90.2	60	179.4	1.16	67.7	18.3
4	92.5	72	189.9	1.34	74.6	17.6
6	93.2	79	190.1	1.26	80.2	17.6
8	96.2	84	216.8	1.12	97.9	16.3
10	95.0	92	225.6	1.17	80.2	15.8

Table 3. Mechanical properties of PVA/PAA/sepiolite nanocomposite films.

Sepiolite content / wt. %	Young's modulus / MPa	Tensile strength / MPa	Elongation at break / %	Energy at break / MJ m⁻³
0	111.0 ± 17.7	19.0 ± 1.3	329.0 ± 26.6	1002.4 ± 53.0
2	177.9 ± 8.1	25.5 ± 1.9	314.2 ± 54.5	1192.4 ± 299.9
4	288.6 ± 22.5	28.8 ± 1.7	182.4 ± 25.3	869.6 ± 94.5
6	432.9 ± 76.6	38.7 ± 1.6	185.7 ± 5.9	1227.1 ± 69.5
8	474.2 ± 73.4	34.4 ± 0.6	183.0 ± 18.0	1126.6 ± 78.0
10	216.4 ± 2.0	16.1 ± 1.3	101.2 ± 2.9	261.7 ± 17.1

Table 4. Mechanical properties of PVA/PAA/sepiolite nanocomposite foams.

Sepiolite content / wt. %	Young's modulus / MPa	Tensile strength / MPa	Elongation at break / %	Energy at break / MJ m⁻³
0	29.9 ± 3.4	0.85 ± 0.02	14.8 ± 0.9	1.62 ± 0.03
2	12.8 ± 2.1	0.54 ± 0.03	18.9 ± 0.6	1.39 ± 0.16
4	10.9 ± 0.8	0.37 ± 0.02	23.7 ± 1.4	1.38 ± 0.21
6	14.9 ± 0.8	0.44 ± 0.01	12.7 ± 0.2	0.70 ± 0.06
8	5.6 ± 0.5	0.22 ± 0.001	24.2 ± 5.4	0.92 ± 0.08
10	9.6 ± 0.7	0.32 ± 0.002	11.2 ± 0.1	0.47 ± 0.01

Highlights

- Novel PAA-crosslinked PVA/sepiolite nanocomposite scaffolds were prepared for the first time.
- The nanocomposite scaffolds were highly porous with interconnected structures and exhibited good mechanical properties, demonstrating potential for further developed as bone scaffolds.
- The effects of sepiolite nanofibres on the structure and properties of the crosslinked PVA scaffolds were investigated in detail.
- The presence of sepiolite increased the strength, stiffness and toughness of the crosslinked PVA film simultaneously, demonstrating effective reinforcement in the solid material that constructs the scaffold.